Magnetic alignment of short carbon fibres in curing composites

Jacopo Ciambella[a,b,*], David C. Stanier[b], Sameer S. Rahatekar[b]

[a] *Dipartimento di Ingegneria Strutturale e Geotecnica*
Sapienza Università di Roma, Via Eudossiana 18, 00184 Rome, Italy
[b] *Advanced Composites Centre for Innovation and Science*
University of Bristol, University Walk, BS8 1TR, Bristol, United Kingdom

Abstract

Alignment of magnetic particles into a viscous fluid by a homogeneous magnetic field has been studied both experimentally and theoretically, but very few studies have investigated the effects of viscosity changes on the capability of achieving complex fibre assemblies in composite materials. In this paper, we study the alignment of short carbon fibres into a viscous matrix whose viscosity is made dependent on the time, in order to simulate the curing process of the composite. A simple model is derived which gives the evolution of fibre position and orientation in terms of the external field and shows good agreement with the experimental evidence on nickel coated carbon fibres embedded in PDMS. The model is used to predict the fibre distribution at curing and hence could be a useful tool to predict the mechanical, electrical and magnetic properties of the composite. A closed form expression of the minimum magnetic field intensity necessary to achieve the

*Corresponding author
Email addresses: jacopo.ciambella@uniroma1.it (Jacopo Ciambella), david.stanier@bristol.ac.uk (David C. Stanier), sameer.rahatekar@bristol.ac.uk (Sameer S. Rahatekar)

desired orientation is derived in terms of the magnetic and geometric properties of the fibres. This equation can be used to guide experiments, and offers a way to discriminate which matrix/fibre configuration can be most proficiently used to have a highly ordered composite.

keywords: A. Fibre; B. Magnetic Properties; B. Cure Behavior; C. Analytical Modelling; E. Assembly

1. Introduction

The requirement for increasingly innovative and lightweight structural solutions has driven the development of anisotropic and hierarchical material architectures, due to the large design space they provide. The outstanding mechanical properties of such materials are typically a result of mimicking the features seen in nature where the self-assembly of hierarchical structures is often used to achieve shape changes upon external stimuli [2]: hydration triggered shape change is often seen in plants whereas humidity driven deformation is achieved in pinecones by restricting swelling or shrinkage in the direction of the reinforcing fibrils [7]. The main difficulty for designers to artificially mimic this behaviour is arranging the fibres in such a configuration so that the performance of the material is improved without drastically increasing the cost.

Self-assembly of fibres has been the focus of much research, with the proposal of many different mechanisms including shear [19], electrical [24], ultrasonic [25] and magnetic alignment [27, 32]. The use of magnetic alignment in particular has gained considerable interest due to several advantages

over the other techniques [23]. First of all, magnetic forces are contactless volume forces which do not produce any chemical alteration in the material and allow the remote orientation of anisotropic particles in 3D spatial configurations [20, 26]. Second, permanent magnets and electromagnets are nowadays readily available and produce strong enough fields to orient the reinforcements and eventually actuate the composite [28]. Finally, compared to electric fields, magnetic fields are not sensitive to surface charge and pH [23].

Erb et al. [6] have researched the effect of particle size and magnetic field strength to achieve a uniform alignment of rod-like and platelet-like particles in the host matrix. Particles in the size range of 10 μm give the optimum response, as these only require a very low magnetic field, less than 2 mT, in order to align them effectively in the host matrix. On the contrary, particles on the nanoscale and particles greater than a few micrometres require a higher magnetic torque to align them. This is due to the thermal forces dominating at smaller scales and gravitational forces dominating for much larger particles. This has been observed for nanoparticles by Takeyama et al.[30], showing that a pulsed magnetic field strength in the region of 40 T was required to obtain good alignment of single wall carbon nanotubes in a sodium dodecyl sulphate surfactant. Further studies [12, 4, 3] corroborate this data, showing that a magnetic field in excess of 10 T can achieve good alignment at room temperature, and as the magnetic field strength increases the alignment becomes more effective.

Once the fibres are aligned to the magnetic field lines they can in turn offer control of the material properties, such as the mechanical performance

[28], thermal stability [4, 11], energy dissipation [3], electrical conductivity [18, 22, 17] and even magnetic actuation [14, 28]. However, the performance of the material depends critically on the degree of orientation; which is in turn dependent not only on the magnetic field strength applied but also on the size, shape, volume [6] and magnetic properties of reinforcing filler used, as well as the curing rate and viscosity of the matrix [1]. Therefore, accurate manufacturing requires the ability to predict the orientation of the dispersion of fibres within the host matrix; wherein the limiting factor to the manufacture is the effect of curing and its associated increase in viscosity with time.

Typically the focus involves the use of fibres dispersed into a liquid solution and oriented by homogeneous fields [13, 12, 16] as this results in a homogeneous dispersion of fibres (in this case: torque is applied to rotate the fibre, but no translation of the fibre takes place). However, an understanding of the effects of the changing viscosity during the curing phase would be beneficial to have an accurate estimate of the final distribution that can be achieved within the composite and select the optimal configuration in terms of matrix/fibre.

This work is driven by the need for a simple tool for the prediction of oriented fibres in solution, which is becoming an increasingly important area of research as the need for highly optimised structures continues to develop [10]. The introduced model is equally applicable to the prediction of diamagnetic or paramagnetic materials, and in fact comparisons of the model are made to experimental data on nickel-coated carbon fibres suspended in a PDMS matrix by considering an initially random and homogeneous distribu-

tion of fibres. It is anticipated that the consideration of a non-homogeneous magnetic field will drive further innovation into novel engineering materials through self-assembly.

The structure of the paper is as follows. In Sect. 2, the general theory driving the alignment of magnetic particles into a matrix with increasing viscosity is presented. In Sect. 3 the procedure followed to produce and characterise the materials is described and in Sect. 4 the predicting capabilities of the proposed model in comparison to the experimental results are discussed and some of the key features of the model are illustrated. Conclusions are drawn in Sect. 5.

2. Theory

This section describes the the motion of a rigid fibre made of magnetic material embedded into a viscous fluid and subjected to an external magnetic field. For the sake of generality, the 3D theory is here introduced whereas in the next section the model is applied to the case where fibres and magnetic field lie in the same plane effectively reducing the problem to a 2D one. The fibre has a cylindrical shape which **is** approximated as a prolate spheroid with characteristic half-lengths ℓ and w ($\ell > w$), aspect ratio $a_r = \ell/w$ and volume $\nu = 4/3\,\pi w^2 \ell$; the direction of the main axis given by the unit vector $\vec{n}$ (see Fig. 1).

The application of an external magnetic field induces a magnetisation $\vec{M}$ in the fibre due to the weak magnetic dipole moments imposed upon the molecular alignment by the magnetic field. Assuming a linear dependence of the magnetisation upon the field and an arbitrary angle of the fibre with the

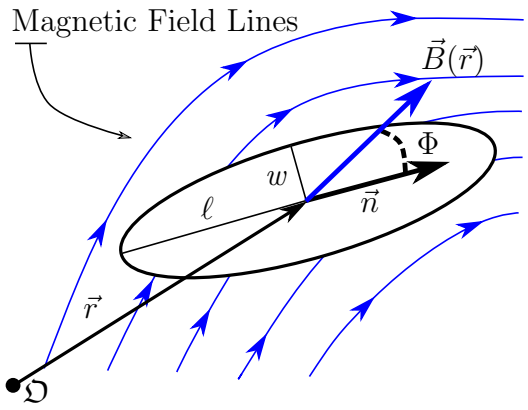

Figure 1: Schematic representation of an ellipsoidal fibre with principal axis $\vec{n}$ embedded into a non-homogeneous magnetic field $\vec{B}(\vec{r})$. $\vec{r}$ is the position vector with respect to a fixed reference frame, w and ℓ the dimensions of the two main axes of the fibre.

direction of $\vec{B}$, the magnetisation $\vec{M}$ and the magnetic energy Ψ of the fibre can be defined by (see [29])

$$\vec{M} = \chi_{m\perp}\mu_0^{-1}\vec{B} + \chi_a\,\mu_0^{-1}(\vec{n}\otimes\vec{n})\vec{B} \tag{1}$$

$$\Psi = -\frac{1}{2}(1+\chi_{m\perp})\mu_0^{-1}(\vec{B}\cdot\vec{B}) - \frac{1}{2}\chi_a\,\mu_0^{-1}(\vec{n}\cdot\vec{B})^2 \tag{2}$$

where $\vec{n}$ is the unit vector indicating the direction of the fibre, μ_0 is the permeability of the vacuum and $\chi_a = \chi_{m\parallel} - \chi_{m\perp}$ is known as *anisotropic magnetic susceptibility* whilst the coefficients $\chi_{m\parallel}$ and $\chi_{m\perp}$ denote the magnetic susceptibilities parallel and perpendicular to the main axis of the fibre[1]. The symbol $\otimes$ indicates the dyadic product between vectors, i.e., $(\vec{a}\otimes\vec{b})_{ij} = a_i\,b_j$, whereas $\cdot$ denotes the scalar product. In deriving Eq. (1), the effect of the demagnetisation field produced on the fibre is assumed to be small that is

[1]In SI units, χ_a, $\chi_{m\parallel}$ and $\chi_{m\perp}$ are all dimensionless quantities.

the effect produced by the presence of the fibres on the external field can be neglected [21].

The anisotropic susceptibility χ_a is, in general, a complex function of both the magnetic properties of the constituent material and the geometric properties of the fibre. Materials with a positive χ_a are called *paramagnetic* and for them, the last term in the magnetic energy is minimised when the fibre and the magnetic field are parallel. All the materials constituted by atoms that have an odd number of electrons will have a magnetic moment and will therefore be paramagnetic. Some atoms with an even number of electrons have a permanent magnetic moment because inner electron shells are unfilled; examples of such atoms are Cr, Al, K, W, and Gd [21]. On the contrary, if $\chi_a < 0$, the energy attains its minimum when the fibre and the magnetic field are perpendicular; such behaviour is observed in H_2, N_2, Ar, Cu, Ag and Pb which are called *diamagnetic* materials[2].

The external actions on the fibre are the magnetic force $\vec{F} = -\nu\nabla\Psi$ and torque $\vec{T} = \nu(\vec{M} \times \vec{B})$ on the fibre and the hydrodynamic drag (ν is the volume of the fibre). If the solution within which the fibres are dispersed has a viscosity that changes with time, e.g., a curing composite, the equation of motion will depend upon the rate of changes of the viscosity. In particular, an empirical expression used in the literature to describe the viscosity of

[2]A different effect is observed in *ferromagnetic* materials for which the relationship between the applied field and the magnetisation is highly nonlinear: even a small magnetic field applied to a ferromagnet can result in its developing a large magnetization [21]. Only three elements, i.e., Co, Fe and Ni are ferromagnetic at room temperature.

curing epoxy is [5, 1, 15]

$$\eta(t) = \eta_0 \, e^{t/\tau_c} \tag{3}$$

where τ_c represents the time at which the viscosity of the solution is e times larger than its initial value η_0 and can be easily determined experimentally. Other expressions of the time-dependent viscosity are possible but it is shown that an accurate description of the system under consideration can be achieved with (3). In any case, changing (3) would not change the subsequent analysis.

The following equations of particle motion [31] in terms of the translational velocity $\vec{v}$ and the rotational velocity $\vec{\omega}$ around the secondary axis are derived

$$\begin{cases} \vec{v} = \left[d_{\parallel}^{-1}(\vec{n} \otimes \vec{n}) + d_{\perp}^{-1}(I - \vec{n} \otimes \vec{n}) \right] \vec{F} \\ \vec{\omega} = d_{\theta}^{-1}(I - \vec{n} \otimes \vec{n}) \vec{T} \end{cases} \tag{4}$$

where $d_{\parallel}$ and $d_{\perp}$ are the translational drag coefficients, and d_{θ} the rotational drag coefficients around the secondary axis and I is the identity operator. In Eq. (4_2) we have deliberately ignored the rotation and the corresponding torque around the primary axis since it is of no interest to the present analysis.

By accounting for Eq. (3) and using the defintion of magnetic force, i.e., $\vec{F} = -\nu \nabla \Psi$, Eq. (4.1) can be rewritten as

$$\frac{d\vec{r}}{dt} = -\nu \, e^{-t/\tau_c} \left[(d_{\parallel}^{0})^{-1}(\vec{n} \otimes \vec{n}) + (d_{\perp}^{0})^{-1}(I - \vec{n} \otimes \vec{n}) \right] \nabla \Psi \, , \tag{5}$$

where as the defintion of magnetic torque, i.e., $\vec{T} = \nu(\vec{M} \times \vec{B})$, and the relationship $d\vec{n}/dt = \vec{\omega} \times \vec{n}$, allow us to compute Eq. (4.2) as

$$\frac{d\vec{n}}{dt} = \vec{\omega} \times \vec{n} = d_{\theta}^{-1}(\vec{T} \times \vec{n}) = \tau_o^{-1} \, e^{-t/\tau_c} (\vec{n} \cdot \vec{b}) \, [I - \vec{n} \otimes \vec{n}] \, \vec{b} \, . \tag{6}$$

In previous equations, $d_{\parallel}^0$, $d_{\perp}^0$ and d_{θ}^0 are the drag coefficients evaluated with respect the initial viscosity η_0; $\vec{b} = \vec{B}/B_0$ is the magnetic field vector normalised to a reference value B_0. The normalisation coefficient B_0 is taken as the average value of the magnetic field over a reference volume Ω_r, $B_0 = \frac{1}{\Omega_r}\int_{\Omega_r}\sqrt{\vec{B}\cdot\vec{B}}\mathrm{d}\Omega_r$ that corresponds, for a uniform magnetic field, to its intensity, i.e., $B_0 = \|\vec{B}\|$.

The scalar coefficients $d_{\parallel}^0$, $d_{\perp}^0$ and $d_{\theta\perp}^0$ which appear in Eqs. (5)-(6) can be calculated as quasistatic values of Stokes flow around a spheroid particle (see for instance [9, 24]). The drag on a spheroid with aspect ratio $a_r \gg 1$ embedded into a fluid with viscosity η_0 is

$$d_{\parallel}^0 \approx \frac{4\pi\eta_0\,\ell}{\ln(2\,a_r) - 1/2}, \quad d_{\perp}^0 \approx \frac{8\pi\eta_0\,\ell}{\ln(2\,a_r) + 1/2}, \quad d_{\theta}^0 \approx \frac{8\pi\eta_0\,\ell^3}{3\,[\ln(2\,a_r) - 1/2]} \tag{7}$$

for motions parallel $d_{\parallel}^0$, perpendicular $d_{\perp}^0$ to the primary axis of the spheroid and for the rotation about an axis perpendicular to the primary axis d_{θ}^0.

The time constant τ_o in (6) is the characteristic time that guides the orientation of a fibre embedded into a solution with viscosity η_0 and subjected to the action of a uniform magnetic field B_0; its expression can be derived from (6) and (7) as

$$\tau_o = \frac{\mu_0}{\chi_a\,B_0^2}\,\frac{d_{\theta}^0}{\nu} = \frac{\mu_0}{\chi_a\,B_0^2}\,\frac{2\,a_r^2\,\eta_0}{\ln\left(2\,a_r\right) - 1/2}\,, \tag{8}$$

and depends on the geometry of the fibre, i.e., a_r, its magnetic properties, i.e., χ_a and the viscosity of the matrix, i.e., η_0.

Standard models, e.g., [12], use a susceptibility independent of the fibre aspect ratio which implies τ_o to be monotonically increasing with a_r, i.e., longer fibres take more time to orient due to the increased drag. However, experimental data collated by the authors on Ni-coated CF, and shown in the

next section, suggest the opposite behaviour, longer fibres aligning quickly towards the magnetic field lines, which implies , χ_a to increase with the fibre a_r.

The solution of (5)-(6), which is a system of nonlinear PDEs, is not an easy matter and in fact an analytical solution is recovered only for a homogeneous field. Such a case has been already dealt with in [14, 6] where a constant viscosity of the embedding fluid was assumed; however, here the solution for a time varying viscosity is derived and it is shown that it can more accurately describe the case of a curing composite. For the sake of simplicity, we restrict our attention to the case of a homogeneous external magnetic field whose orientation does not change with time. In this situation, the equation in (5) vanishes ($\|\nabla\Psi\| = 0$). By using the following relationship

$$\vec{n} \times \frac{d\vec{n}}{dt} = \vec{n} \times \vec{\omega} \times \vec{n} = \frac{d\Phi}{dt}\vec{k}, \tag{9}$$

between the derivative of the orientation vector $\vec{n}$ and the angular velocity $\vec{\omega} = d\Phi/dt\,\vec{k}$, assumed here perpendicular to the plane containing both the fibre and the magnetic field lines, the remaining governing equation (6) can be expressed in dimensionless form as

$$\frac{\mathrm{d}\Phi}{\mathrm{d}t_r} = -\frac{1}{2}e^{-\gamma\, t_r}\sin(2\Phi)\,, \tag{10}$$

where Φ is the relative angle between the fibres and the magnetic field, and γ is the ratio between the orientation characteristic time τ_o and the characteristic curing time τ_c, i.e., $\gamma = \tau_o/\tau_c$. In (10) $t_r := t/\tau_o$ represents the normalised time.

The fact that, under the action of a uniform field, fibres rotate but do not translate makes the use of a homogeneous field advantageous for the

experimentalists; as a result, an initially homogeneous distribution of fibres remains homogeneous under the effect of the external field.

The case of a matrix with constant viscosity is encompassed by the model (10) when $\gamma \to 0$, a case which was already dealt with in [13] and [14]. The solution of Eq. (10) in terms of the initial angle Φ_0 is

$$\tan(\Phi(t_r)) = \tan(\Phi_0)\, e^{\left(\frac{-1+e^{-\gamma\, t_r}}{\gamma}\right)}, \tag{11}$$

which is a useful tool to predict the fibre distribution achieved after a time t_r. In fact, the total number of fibres ΔN oriented at time t_r within an angle $\Delta\Phi$, can be worked out in terms of the distribution function $\rho(\Phi, t_r) := \lim_{\Delta\Phi\to 0} \Delta N/\Delta\Phi$. Hence one has $\rho(\Phi, t_r) = \mathrm{d}N/\mathrm{d}\Phi = (\mathrm{d}N/\mathrm{d}\Phi_0)(\mathrm{d}\Phi_0/\mathrm{d}\Phi)$, which allows the distribution ρ to be obtained from (11). By assuming a random orientation at time $t_r = 0$, then the initial distribution $\mathrm{d}N/\mathrm{d}\Phi_0$ is constant and equal to $1/\pi$. By inverting Eq. (11) and taking the derivative with respect to Φ_0, one obtains the following distribution function ρ ($\int_{-\pi/2}^{\pi/2} \rho\, \mathrm{d}\Phi = 1$)

$$\rho(\Phi, t_r, \gamma) := \frac{1}{\pi}\frac{\mathrm{d}\Phi_0}{\mathrm{d}\Phi} = \frac{1}{\pi}\frac{e^{\frac{1+e^{-\gamma\, t_r}}{\gamma}}\sec(\Phi)^2}{e^{\frac{2e^{-\gamma\, t_r}}{\gamma}} + e^{\frac{2}{\gamma}}\tan(\Phi)^2} \tag{12}$$

which at curing, i.e., $t_r \to +\infty$, reduces to

$$\rho(\Phi, \gamma) = \frac{1}{\pi}\frac{e^{\frac{1}{\gamma}}\sec^2(\Phi)}{1 + e^{\frac{2}{\gamma}}\tan^2(\Phi)}. \tag{13}$$

The function ρ in (12) is plotted in Fig. 2 to show the evolution of the fibre orientation for two values of the parameter γ, i.e., for two different curing times of the composite. In both cases, the fibres have at time $t_r = 0$ the random orientation represented by a straight line. For $\gamma = 5$, the characteristic orientation time τ_o is larger than the characteristic curing time

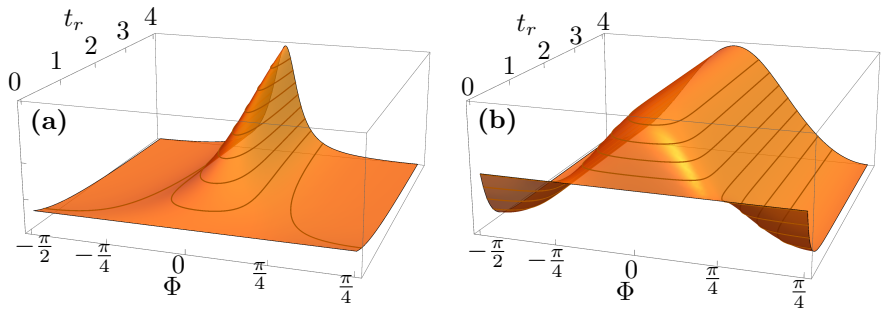

Figure 2: Evolution of the fibre orientation distribution of the fibre (12) for $\gamma = 0.5$, i.e., a slowly curing matrix (a) and $\gamma = 5$, i.e., fast curing matrix (b). A random orientation of the fibres is assumed at $t_r = 0$.

and in fact the composite solidifies before the fibres have the possibility to fully orient with the magnetic field lines. As such, the final distribution has a much larger orientation spread than the case of $\gamma = 0.5$ for which the curing time doubles the orientation time.

The probability p_ϕ of having a fibre with an orientation of $\pm\phi$ at time t_r is given by

$$p_\phi := \int_{-\phi}^{\phi} \rho(\Phi, t_r, \gamma)\, \mathrm{d}\Phi = \frac{2}{\pi}\, \mathrm{atan}\left(\tan(\phi) e^{\frac{1-e^{-\gamma\, t_r}}{\gamma}}\right) \tag{14}$$

whose inversion with respect to the reduced time t_r gives

$$t_r = -\frac{1}{\gamma}\, \ln\left(1 - \gamma\, \ln\left(\frac{\tan(\pi\, p_\phi/2)}{\tan(\phi)}\right)\right) \tag{15}$$

Equation (15) gives the time necessary to achieve an orientation of p_ϕ with a spread in the fibre angles of $\pm\phi$. Certainly, the possibility to achieve such a spread depends upon the ratio γ between the orientation time and the curing time of the composite: large values of γ imply the composite cures too fast to allow the fibres to achieve the desired orientation.

Equation (15) is defined only if the argument of the logarithm is positive, i.e., $\gamma \log(\tan(\pi\phi/2)/\tan(\phi)) < 1$; such a condition gives the maximum value of γ at which the desired orientation is achievable. Correspondingly, by using the definition of $\gamma = \tau_0/\tau_c$ and Eq. (8), it is possible to work out the minimum magnetic field that allows the orientation spread of $\pm\phi$ for p_ϕ of fibres at curing, i.e.,

$$B_{0\,min}^{(p_\phi,\phi)} = \left[\frac{\eta_0\,\mu_0}{\tau_c\,\chi_a}\,\frac{2\,a_r^2}{\ln(2\,a_r)-1/2}\,\ln\!\left(\frac{\tan(\pi p_\phi/2)}{\tan(\phi)}\right)\right]^{1/2}. \tag{16}$$

Apparently, the magnetic field intensity depends upon the curing rate of the composite, i.e., η_0/τ_c, and the magnetic and geometric properties of the fibres. Magnetic fields up to 1 T can be generated in a normal lab environment through the proper assembly of neodymium magnets [28] without using large and complex electromagnets. In this sense, Eq. (16) represents a useful tool to discriminate which materials and fibres can be used to achieve fibre orientations with a reasonably low magnetic field. In Sect. 3 this equation is compared against the experimental data collated by the authors.

The contour plot of this function is shown in Fig. 3 for carbon fibres ($\chi_a = 10^{-4}$) in terms of the curing rate $\dot{\eta}_0 = \eta_0/\tau_c$ and the fibre aspect ratio a_r. The red area in the figure shows the region where the magnetic field is higher than 1 T; any configuration which falls within this area requires fields that cannot be generated by "standard" magnets but requires more complex equipment such as superconducting magnets [13].

3. Material Preparation and Characterisation

The experiments involved dispersing Nickel coated Carbon Fibres (NiCF) into the pre-cure phase of a PDMS solution. The fibres were subsequently

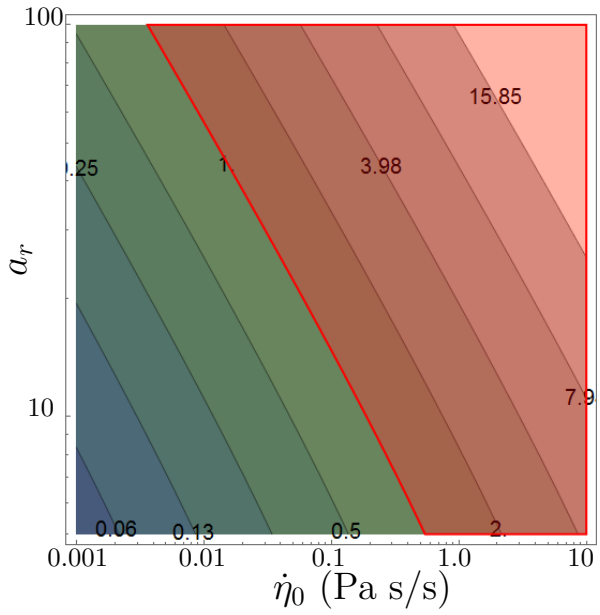

Figure 3: Contour plot of the minimum magnetic field intensity $B_{0\,min}$ to have 90% of the fibres oriented at $\pm 5°$. $B_{0\,min}$ is plotted against the initial curing rate $\dot{\eta}_0 = \eta_0/\tau_c$ and the fibre aspect ratio a_r. The other parameters in Eq.(16) are $\chi_a = 10^{-4}$, $\mu_0 = 4\,\pi \times 10^{-7}$ T m/A. The labels shows the magnetic filed intensity in Tesla. The red area represents the region where B_0 is higher than 1 T, that would require expensive experimental setup.

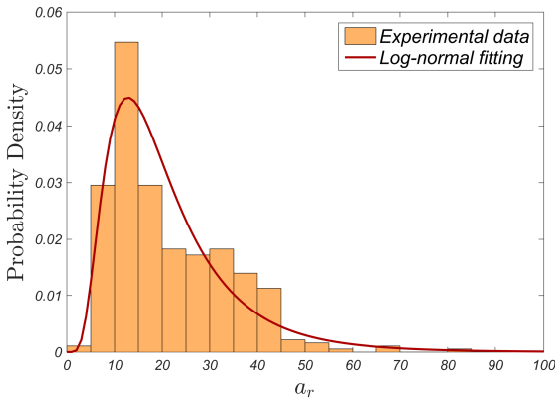

Figure 4: Distribution of the fibre aspect ratio a_r, fitted to a log-normal distribution for > 600 fibres ($\mu = 2.89, \sigma = 0.58$). The corresponding mean value is $\overline{a_r} = 21.3$.

oriented in the presence of a homogeneous magnetic field, and their position recorded by optical microscopy.

PDMS (Sylgard 184) was used without further modification. Nickel coated short carbon fibres (40/60 Ni/C, diameter 4.8 μm) were purchased from Marktek Inc. and used as received. The nominal purchased length of the fibres was 0.25 mm, however microscopy indicates a distribution in the fibre length and an actual average fibre length of approximately 0.1 mm (see Fig. 4). This is presumably due to damage to the fibres occurring during manufacturing as evidenced by the SEM images in Fig. 5 where damage to the fibre and to the Ni coating are shown. A carefully weighed quantity of fibres are directly mixed with the base component of PDMS to give 5 wt% of fibres.

The fibres/PDMS mixture was firstly agitated to partially homogenise the mixture, then sonicated for 1 hour and then again agitated. The supernatant was then separated and added to curing dishes in 1g quantities, before curing

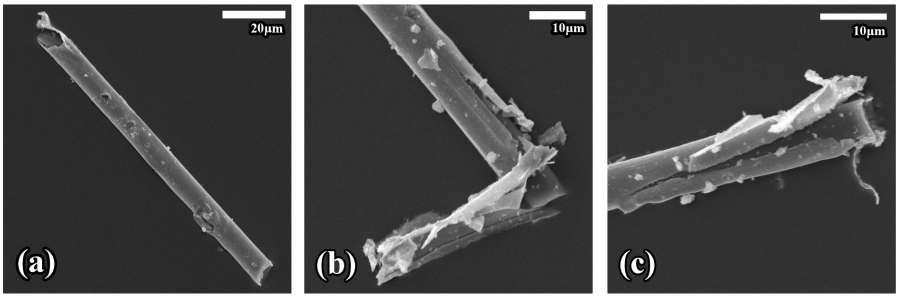

Figure 5: NiC fibres characterisation under SEM showing (a) an intact fibre; (b) broken fibre; (c) broken interface.

agent was added at an approximate ratio of base to hardener of 10:1, with the remaining PDMS residue and NiC sediment cured at room temperature. This residue is burned off at 500^{o}C and weighed to determine the amount of unused NiC fibre material; this allows the fibre concentration of the PDMS specimens to be determined as 2.1 wt%.

The initial working viscosity of the solution is estimated by the manufacturer to be $\eta_0 = 3.5$ Pa s, whereas the characteristic curing time $\tau_c = 180$ min has been estimated from the gelation point of the PDMS. The solution viscosity is expected to be increased by the inclusion of the short fibres, however only a small impact is expected due to the low wt% used.

The petri dish was placed between the plates of an electromagnet (Newport Instruments Electromagnet Type C, 4900 turns on each coil) which generates an approximately homogeneous magnetic field. An image of the electromagnetic setup from above can be seen in Fig.6.

The experimental program consisted of firstly investigating the effect of the viscosity changes on the fibre alignment, thus capturing microscope images (Carl Zeiss Jenavert) of the fibre mixture at time intervals t =

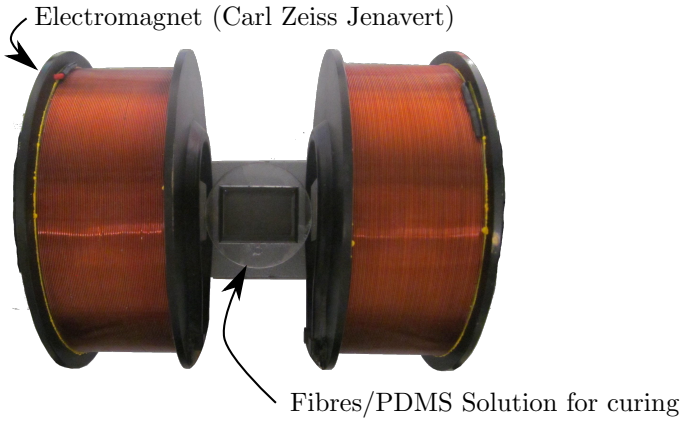

Figure 6: Experimental setup for specimen curing, with the specimen placed directly between the plates of the electromagnet. In this configuration, the electromagnet (mod. Carl Zeiss Jenavert) was able to generate a maximum homogeneous field of 80 mT.

$\{20, 60, 160, 220, 340, 3600\}$ min at a constant field strength of $B_0 = 0.08$ T. After 340 mins the solution was practically cured. The micrographs were subsequently post-processed by the Matlab Image Processing Toolbox (R2012b) to determine the position, orientation and size of the fibres. Each micrograph contained at least six hundred fibres, which has allowed separate treatment of the fibres with different aspect ratios, thus assessing the influence of fibre length on the alignment achieved once cured.

A second investigation was carried out to understand the effect of the magnetic field strength, thus different specimens were placed in magnetic fields of strength $B_0 = \{0.01, 0.03, 0.05, 0.08\}$ T for 1 hour.

4. Results and Discussion

During the curing process, fibres originally randomly dispersed rotate to align with the magnetic field lines. This process is evidenced in Fig. 7

where actual micrographs of the specimen, together with the corresponding fibre orientation distribution, are shown at three different times $t = \{60, 220, 340\}$ min for a specimen subjected to a constant field of 80 mT. Fibres with the lowest aspect ratio, i.e., $10 < a_r < 20$, have the lowest tendency to align with the field lines and, in fact, after 340 min their distribution function has a large spread around the field direction at $\Phi = 0^\circ$. On the contrary, a large number of long fibres with $a_r > 30$ are already oriented after 60 mins and at 340 min the distribution function displays a sharp peak. In terms of the characteristic orientation time τ_o, this corresponds to longer fibres being associated with lower τ_o compared to the shorter ones.

Such behaviour is indeed the opposite of that expected from the definition (8) in which τ_o increases with a_r. However, it is also expected that long fibres have a larger susceptibility compared to the shorter ones, and therefore, χ_a being a measure of the fibre anisotropy, should increase with a_r; such a circumstance indeed explains the behaviour observed in Fig 7.

To further investigate this effect, the distribution functions are compared to Eq. (12) in four different aspect ratio ranges, i.e., $[10-20, 20-30, 30-40, 40-50]$ and the corresponding results shown in Fig. 8. Each curve is obtained by solving, in Matlab (R2012b), a nonlinear least square problem that for each a_r tries to fit the data from the three times $\{60, 220, 340\}$ min.

The quality of the fitting is seen in Fig. 8 with the model closely matching the experimental data at the lowest a_r and giving accurate results at larger aspect ratios except for $t = 60$ min when the model underestimates the portion of oriented fibres. As such, the corresponding characteristic orientation times τ_o will be slightly underestimated. In terms of τ_o, the fitting gives

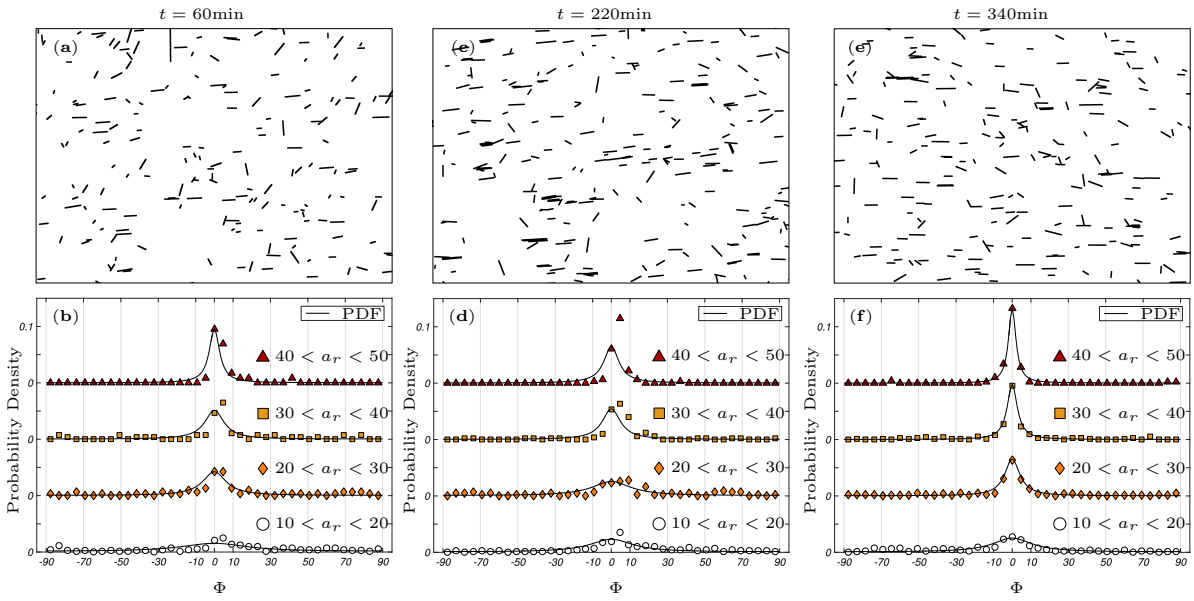

Figure 7: Fibre distribution achieved after 60 mins ((a)-(d)), 220 mins ((b)-(e)) and 340 mins ((c)-(f)) for fibres initially randomly oriented. The continuous lines show the fitting by model (12) carried out at different aspect ratios. Insets (a), (b) and (c) show actual micrographs of a selected portion of the specimen whose contrast is enhanced for illustrative purpose. The specimen was practically cured after 340 mins.

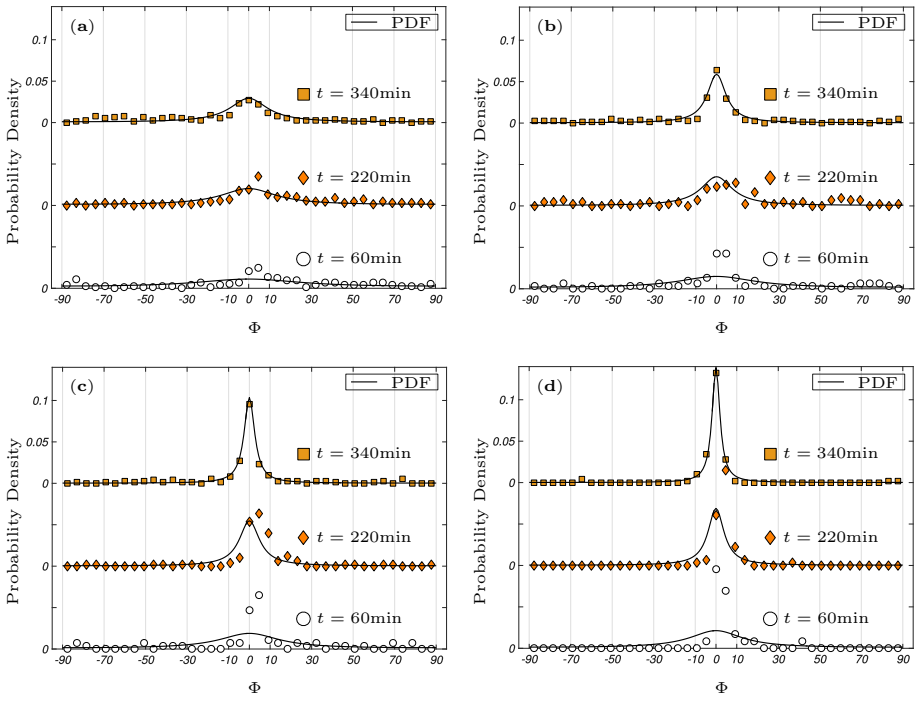

Figure 8: Evolution of fibre distribution with time during the curing phase of the composite for: $10 < a_r < 20$ (a), $20 < a_r < 30$ (b), $30 < a_r < 40$ (c), $40 < a_r < 50$ (d). The fibres were subjected to a constant magnetic field of 80 mT.

$\{90, 62, 52, 47\}$ min for fibres with average aspect ratios of $\{15, 25, 35, 45\}$, respectively. From these values and by inverting Eq. (8), one could evaluate the anisotropic susceptibility whose values are shown in Fig. 9 in terms of fibres a_r: χ_a has a quadratic dependence on the fibre a_r and passes from about $2.5{\times}10^{-3}$ for fibres with an average aspect ratio of 15 to $2.5{\times}10^{-2}$ for an average aspect ratio of 45. The fitting function in Fig. 9 is $\chi_a = \alpha\, a_r^2 + \beta$ with $\alpha = 1.702 \times\ 10^{-5}$ and $\beta = -1.492 \times\ 10^{-3}$. These values are at least one order of magnitude higher than the one reported in previous studies for neat CF and confirm our previous estimate carried out with a different technique [28]. Such a high value of the anisotropic susceptibility highlights the positive effect of the Nickel coating on the magnetic properties of the CF, that allows them to be oriented with a low intensity field easily generated in a lab environment with inexpensive magnets (compared, for instance, to the 8 T cryogen-free superconducting magnet used in [13] to orient neat CF).

The effects of the magnetic field intensity have also been investigated and the corresponding results shown in Figs. 10-12.

In particular, Fig. 10 displays the effect of increasing the magnetic field from 10 mT to 80 mT for fibres with different aspect ratios; each of the ranges were selected to have at least one hundred fibres in the statistics. As expected, the shortest fibres are associated with the highest τ_o and, in fact, even the strongest field, i.e., 80 mT, does not produce any significant alignment after 1 h. On the other hand, a_r three times larger guarantees a much higher alignment with 80 mT and a lower spread in the distribution function. The continuous curves in the figure represent the results of the fitting obtained by solving a nonlinear least square problem for each orientation range

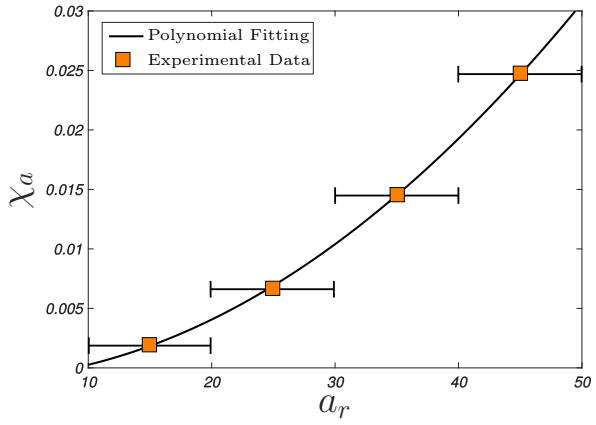

Figure 9: Magnetic susceptibility of the fibres χ_a in terms of the aspect ratio a_r obtained from Eq. (8) and the data in Fig. 8. The fitting function is $\chi_a = \alpha\ a_r^2 + \beta$ ($\alpha = 1.702 \times\ 10^{-5}$, $\beta = -1.492 \times\ 10^{-3}$).

and for all the field intensities considered.

Once the values of τ_o are known, the probability of having a certain orientation can be evaluated by Eq. (14) and the comparison to the experimental data is made in Fig. 11. The model is able to describe the qualitative behaviour seen in the experimental data with larger errors at the lowest field intensities when the number of oriented fibres is lower and the experimental/post-processing errors potentially larger. As expected, the probability of achieving the desired orientation increases with the field intensity; however, for low aspect ratio fibres such an increase is rather marginal and suggests the use of a high field to be an unnecessary complication of the experimental set-up.

Finally, Eq. (16) is used to compute the minimum magnetic field necessary to have 30% of fibres oriented with a spread of $\pm$ 5° at curing. As per the

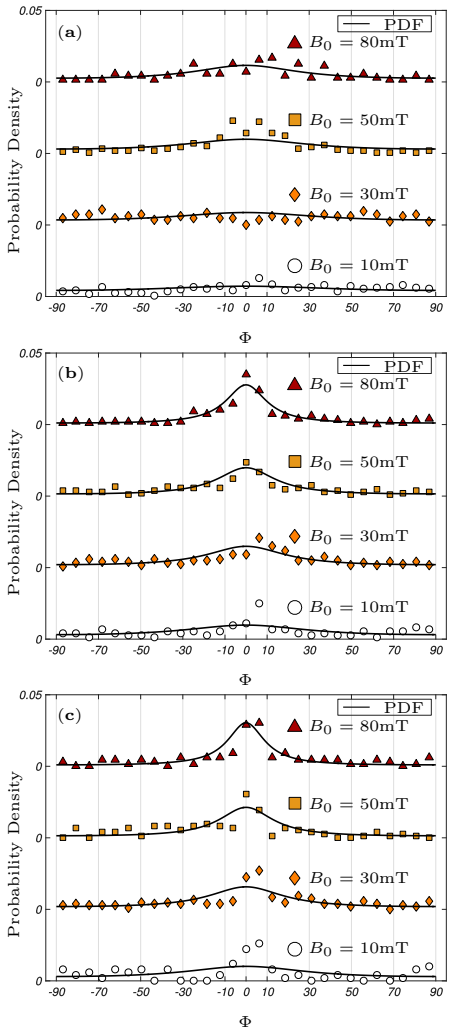

Figure 10: Fibre distribution achieved after 1 h for different field intensities and three different aspect ratio ranges: 5-8 (a), 10-13 (b) and 20-23 (c). The data is fitted against Eq. (12).

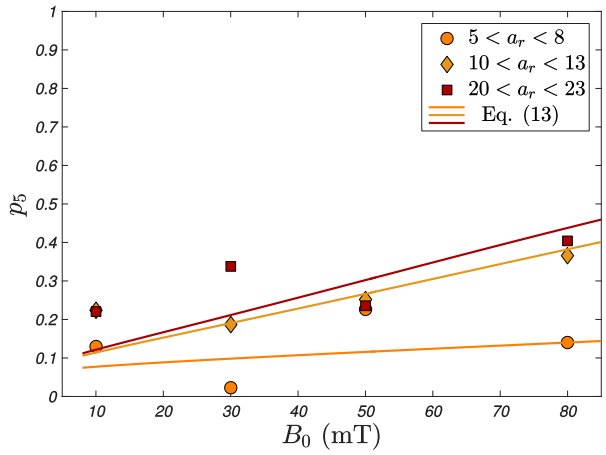

Figure 11: Probability of having fibre oriented at ± 5° after 1 h. **The experimental results *(dots)*** compared to Eq. (14) **(*solid lines*)** for different aspect ratios of the fibres.

results in Fig. 12, the minimum field monotonically decreases for increasing a_r of the fibre within the investigated range. As such, longer fibres would require a lower field to achieve the desired orientation. In particular, it is seen from the figure that within the investigated a_r range, i.e., $10 < a_r < 50$, even the lowest field intensity, 10 mT, is enough to achieve the desired orientation.

The dependence of the fibre geometry/properties on the magnetic orientation in solution has previously been illustrated [6, 30]. However, by considering the effects of the fibre geometry on the viscous and magnetic forces, as well as the effects of viscosity changes in the solution, the model is able to provide a clearer picture of the experimentally determined fibre assembly in the cured state. In turn, this makes it a useful tool to determine an optimum matrix/fibre combination, as well as predict the mechanical, electrical and magnetic properties of the composite that can be strongly linked to the anisotropy of the constituents.

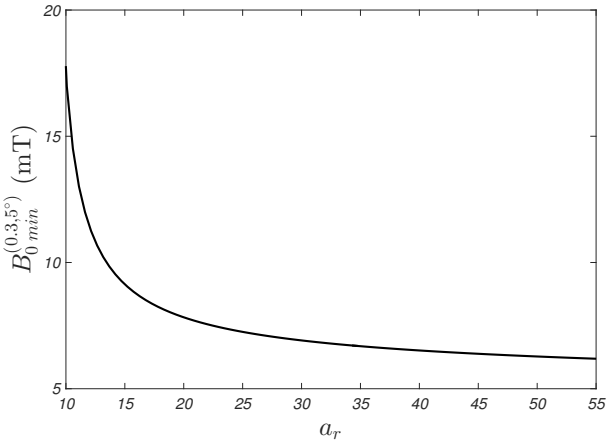

Figure 12: Minimum magnetic field necessary to have 30% of the fibres oriented at $\pm$ 5°.

5. Conclusions

In this paper, the possibility of orienting short carbon fibres in an elastomeric matrix during the curing process of a composite has been studied theoretically and experimentally. The evolution of the fibre orientation was evaluated in terms of time, fibre aspect ratio and magnetic field intensity. The data obtained by optical microscopy has been post-processed by Digital Image Correlation routines and the results have been used to derive a simple model to predict the evolution of fibre distribution with time. One of the peculiarities of the model is that it allows the minimum magnetic field necessary to achieve a certain orientation to be estimated. It is shown that this quantity depends on the curing rate of the matrix, defined as the the initial viscosity over the curing time, as well as on the geometric and magnetic properties of the fibre.

By comparing the model to the experimental data on Nickel coated CF, the anisotropic susceptibility of the fibres was estimated to be at least one

order of magnitude higher than the one reported in previous studies for neat CFs for all aspect ranges considered. This finding indeed confirms the results of other experiments carried out with a different technique in [28]. Moreover, it is shown that anisotropic susceptibility increases quadratically with the fibre aspect ratio within the investigated range ($10 <$ aspect ratio < 50). Although the matrix offers a higher resistance to orient long fibres, the increase in the magnetic susceptibility prevails and allows the longer fibres to be oriented faster as confirmed by other literature results [12]. As a consequence, the magnetic field necessary to achieve a certain orientation is reduced.

In conclusion, the model is intended to provide the experimentalists with a simple yet effective tool capable of estimating, for a given matrix/fibre system, the minimum magnetic field necessary to achieve a certain degree of orientation of the fibre, the time necessary to achieve such an orientation and the fibre distribution at curing. The latter information can be used in conjunction with other models, e.g., [8], to predict the mechanical properties of this highly ordered composite material.

Acknowledgements

This work was supported by the Engineering and Physical Sciences Research Council through the EPSRC Centre for Doctoral Training in Advanced Composites for Innovation and Science [grant number EP/G036772/1]. JC acknowledges the support of the Italian Group of Mathematical Physics (GNFM-INdAM) under the Grant "Progetto Giovani 2016". The authors wish to thank the anonymous reviewers for their useful suggestions.

References

[1] J M Barton, D C L Greenfield, and K A Hodd. Some effects of structure on the cure of glycidylether epoxy resins. *Polymer*, 33(6):1177–1186, 1992.

[2] I Burgert and P Fratzl. Actuation systems in plants as prototypes for bioinspired devices. *Philosophical transactions. Series A, Mathematical, physical, and engineering sciences*, 367(1893):1541–57, 2009.

[3] E Camponeschi, R Vance, M Al-Haik, H Garmestani, and R Tannenbaum. Properties of carbon nanotubepolymer composites aligned in a magnetic field. *Carbon*, 45(10):2037–2046, 2007.

[4] E S Choi, J S Brooks, D L Eaton, M S Al-Haik, M Y Hussaini, H Garmestani, D Li, and K Dahmen. Enhancement of thermal and electrical properties of carbon nanotube polymer composites by magnetic field processing. *Journal of Applied Physics*, 94(9):6034, 2003.

[5] M R Dusi, C A May, and J C Seferis. Predictive Models as Aids to Thermoset Resin Processing. In A M Clayton, editor, *Chemorheology of Thermosetting Polymers*, volume 227, chapter 18, page 301. ACS Publications, Washington, D.C., acs sympos edition, 1982.

[6] R M Erb, R Libanori, N Rothfuchs, and A R Studart. Composites reinforced in three dimensions by using low magnetic fields. *Science*, 335(6065):199–204, 2012.

[7] R M Erb, J S Sander, R Grisch, and A R Studart. Self-shaping composites with programmable bioinspired microstructures. *Nature communications*, 4:1712, 2013.

[8] S-Y Fu and B Lauke. The elastic modulus of misaligned short-fiber-reinforced polymers. *Composites science and technology*, 3538(97):389–400, 1998.

[9] J Happel and H Brenner. *Low Reynolds number hydrodynamics*. Kluwer Academic Publishers, 1983.

[10] B C Kim, P M Weaver, and K Potter. Computer aided modelling of variable angle tow composites manufactured by continuous tow shearing. *Composite Structures*, 129:256–267, 2015.

[11] K Kim and J Kim. Magnetic aligned aln/epoxy composite for thermal conductivity enhancement at low filler content. *Composites Part B: Engineering*, 93:67 – 74, 2016.

[12] T Kimura. Study on the Effect of Magnetic Fields on Polymeric Materials. *Polymer Journal*, 35(11):823–843, 2003.

[13] T Kimura, Y Umehara, and F Kimura. Fabrication of a short carbon fiber/gel composite that responds to a magnetic field. *Carbon*, 48(14):4015–4018, 2010.

[14] T Kimura, Y Umehara, and F Kimura. Magnetic field responsive silicone elastomer loaded with short steel wires having orientation distribution. *Soft Matter*, 8(23):6206, 2012.

[15] J.M. Laza, C.a. Julian, E. Larrauri, M. Rodriguez, and L.M. Leon. Thermal scanning rheometer analysis of curing kinetic of an epoxy resin. I. An Anhydride as curing agent. *Journal of Applied Polymer Science*, 71:1239–1245, 1999.

[16] R Libanori, R M Erb, and A R Studart. Mechanics of platelet-reinforced composites assembled using mechanical and magnetic stimuli. *ACS applied materials & interfaces*, 5(21):10794–10805, 2013.

[17] T.L. Makarova, P. Geydt, I. Zakharchuk, E. Lahderanta, A.A. Komlev, A.A. Zyrianova, M.A. Kanygin, O.V. Sedelnikova, V.I. Suslyaev, L.G. Bulusheva, and A.V. Okotrub. Correlation between manufacturing processes and anisotropic magnetic and electromagnetic properties of carbon nanotube/polystyrene composites. *Composites Part B: Engineering*, 91:505 – 512, 2016.

[18] C A Martin, J K W Sandler, A H Windle, M-K Schwarz, W Bauhofer, K. Schulte, and M S P Shaffer. Electric field-induced aligned multi-wall carbon nanotube networks in epoxy composites. *Polymer*, 46(3):877–886, 2005.

[19] J J Martin, M S Riederer, M D Krebs, and R M Erb. Understanding and overcoming shear alignment of fibers during extrusion. *Soft matter*, 11(2):400–5, 2015.

[20] K Mirica, F Ilievski, A K Ellerbee, S S Shevkoplyas, and G M Whitesides. Using magnetic levitation for three dimensional self-assembly. *Advanced Materials*, 23(36):4134–4140, 2011.

[21] G L Pollack and D R Stump. *Electromagnetism*. Addison Wesley, San Francisco, 2002.

[22] S G Prolongo, B G Meliton, G Del Rosario, and A Ureña. New alignment procedure of magnetiteCNT hybrid nanofillers on epoxy bulk resin with permanent magnets. *Composites Part B: Engineering*, 46:166–172, 2013.

[23] R S M Rikken, R J M Nolte, J C Maan, J C M van Hest, D Wilson, and P C M Christianen. Manipulation of micro- and nanostructure motion with magnetic fields. *Soft matter*, 10(9):1295–308, 2014.

[24] K Rose, J Meier, G Dougherty, and J Santiago. Rotational electrophoresis of striped metallic microrods. *Physical Review E*, 75(1):011503, 2007.

[25] M-S Scholz, B W Drinkwater, and R S Trask. Ultrasonic assembly of anisotropic short fibre reinforced composites. *Ultrasonics*, 54(4):1015–9, 2014.

[26] D. Shi, P. He, P. Zhao, F. F. Guo, F. Wang, C. Huth, X. Chaud, S. L. Budko, and J. Lian. Magnetic alignment of ni/co-coated carbon nanotubes in polystyrene composites. *Composites Part B: Engineering*, 42(6):1532 – 1538, 2011.

[27] W Shi, R Liang, S Xu, Y Wang, C Luo, M Darwish, and S K Smoukov. Layer-by-layer self-assembly: Toward magnetic films with tunable anisotropy. *Journal of Physical Chemistry C*, 119(23):13215–13223, 2015.

[28] D C Stanier, J Ciambella, and S S Rahatekar. Fabrication and characterisation of short fibre reinforced elastomer composites for bending and twisting magnetic actuation. *Composites Part A: Applied Science and Manufacturing*, 91:168–176, 2016.

[29] I W Stewart. *The Static and Dynamic Continuum Theory of Liquid Crystals*. Taylor & Francis, London, 2004.

[30] S Takeyama, S Nakamura, and K Uchida. Dynamical orientation of carbon nanotubes by pulsed magnetic fields. *Journal of Physics: Conference Series*, 51:446–449, 2006.

[31] M Yamaguchi and Y Tanimoto. *Magneto-Science*. Springer, Berlin, 2006.

[32] F H Zhang, Z C Zhang, C J Luo, I T Lin, Y Liu, J Leng, and S K Smoukov. Remote, fast actuation of programmable multiple shape memory composites by magnetic fields. *Journal of Materials Chemistry C*, 3(43):11290–11293, 2015.